Carbohydrate Polymers 104 (2014) 143–150

Contents lists available at ScienceDirect

Carbohydrate Polymers

journal homepage: www.elsevier.com/locate/carbpol

# Reinforcement of all-cellulose nanocomposite films using native cellulose nanofibrils

Jiangqi Zhao[a], Xu He[a], Yaru Wang[a], Wei Zhang[a,*], Xinxing Zhang[a], Xiaodan Zhang[b], Yulin Deng[b], Canhui Lu[a,*]

[a] State Key Laboratory of Polymer Materials Engineering, Polymer Research Institute at Sichuan University, Chengdu 610065, China
[b] School of Chemical and Biomolecular Engineering and IPST at GT, Georgia Institute of Technology, Atlanta 30332-0620, GA USA

ARTICLE INFO

*Article history:*
Received 28 September 2013
Received in revised form
27 December 2013
Accepted 5 January 2014
Available online 10 January 2014

*Keywords:*
All-cellulose composites
Cellulose nanofibrils
Mechanical properties
Optical transparency
Self-reinforcement

ABSTRACT

All-cellulose nanocomposite films were prepared using native cellulose nanofibrils (CNFs) as fillers and lithium chloride/N,N-dimethylacetamide (LiCl/DMAc) dissolved regenerated cellulose as the matrix. The CNFs, with diameters in the range of 15–40 nm were obtained by combined physical methods of ultrasonic treatment and high shear homogenization. The morphology, structure, and properties of the nanocomposite films were characterized by scanning electron microscope (SEM), X-ray diffraction (XRD), optical transmittance, thermal gravimetric analysis (TGA), and mechanical testing. The nanocomposite films exhibited good optical transparency, thermal stability, and remarkably enhanced mechanical properties compared to the regenerated cellulose matrix. By varying the CNFs content, the tensile strength of the nanocomposite films increased from 61.56 MPa to 99.92 MPa and the Young's modulus increased from 0.76 GPa to 4.16 GPa. This work provided a promising pathway for manufacturing high performance and environmental-friendly all-cellulose nanocomposites.



## 1. Introduction

With gradual depletion of fossil fuels, there is growing interest in using more environmentally friendly materials and naturally occurring polymers for new materials (Tonoli et al., 2012). Cellulose is the most abundant renewable and biodegradable polymer on earth (Jayaramudu et al., 2013). Due to its unique properties, such as excellent mechanical properties, nontoxic and environmentally friendly nature, (Sehaqui, Salajkova, Zhou, & Berglund, 2010; Takagi & Asano, 2008), cellulose is becoming more and more important as a renewable resource to replace petroleum-based materials (Cervin et al., 2013). Natural fibers derived from wood (Abraham et al., 2011; Abe & Yano, 2012), cotton (Xiong, Zhang, Tian, Zhou, & Lu, 2012), sugarcane bagasse (Ma, Xue, Yu, & Wang, 2012), coir fiber (Abraham et al., 2013a) and sisal (Madera-Santana, Soto Valdez, & Richardson, 2013) can be added to regenerated cellulose and improve the mechanical properties of resulting composites. Such self-reinforced cellulose composites are bio-based and biodegradable materials (Gao, Yu, Liu, & Chen, 2012). Along with the wide applications of cellulosic composite materials, the all-cellulose composites will constitute an important part in our daily life.

All-cellulose composite was first introduced by Nishino, Matsuda, and Hirao (2004). It was composed of ramie fibers embedded in a matrix of regenerated cellulose. Subsequently, various all-cellulose composites have been prepared by either partial dissolving cellulose fibers or direct incorporating cellulose nanocrystals (CNCs) into a generated cellulose matrix (Gindl-Altmutter et al., 2012; Huber et al., 2012; Vallejos, Peresin, & Rojas, 2012). However, the length/diameter ratios of CNCs are relatively low and their production processes often involve concentrated acid or other harmful chemicals. Recently, native cellulose nanofibrils (CNFs) have been successfully utilized as reinforcing fillers for synthetic polymer matrices (Dagnon, Shanmuganathan, Weder, & Rowan, 2012; Jonoobi, Mathew, Abdi, Makinejad, & Oksman, 2012), biopolymer matrices (Abraham et al., 2013b; Azeredo et al., 2009; Teixeira et al., 2009), as well as inorganic matrices (Tonoli et al., 2013). The CNFs have many unique characteristics such as large length/diameter ratio (Leitner, Hinterstoisser, Wastyn, Keckes, & Gindl, 2007), high mechanical properties (Syverud, Chinga-Carrasco, Toledo, & Toledo, 2011), and the ability to form highly porous meshes (Abraham et al., 2011). It has been reported that the axial modulus of cellulose crystal can be as high as 150 GPa (Sehaqui et al., 2012). At the same nanocellulose concentration, CNFs led to higher strength and modulus compared to CNCs in the composites (Xu et al., 2013). It is also noteworthy that CNFs can be obtained from cellulose fibers via chemical-free physical processes (Chen et al., 2011; Zhao et al., 2013). Therefore, CNFs are

* Corresponding author. Tel.: +86 28 85460607; fax: +86 28 85402465.
*E-mail addresses:* weizhang@scu.edu.cn (W. Zhang), canhuilu@263.net (C. Lu).

0144-8617/$ – see front matter © 2014 Elsevier Ltd. All rights reserved.
http://dx.doi.org/10.1016/j.carbpol.2014.01.007

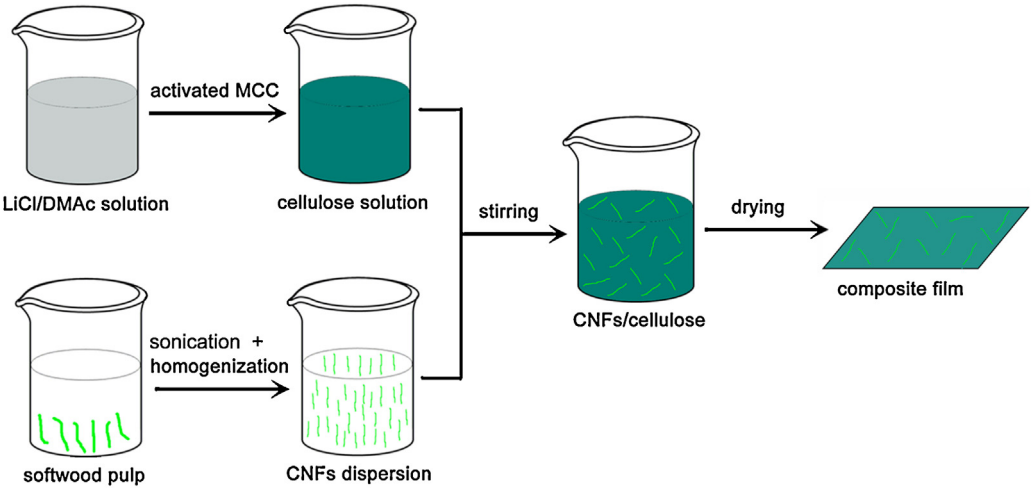


**Fig. 1.** Procedures for manufacturing CNFs reinforced all-cellulose nanocomposites.

very promising as an alternative reinforcement in nanocomposites (Abe, Iwamoto, & Yano, 2007; Abraham et al., 2011).

In this study, the CNFs were used to reinforce all-cellulose nanocomposite films. As far as we know, this is the first demonstration of all-cellulose nanocomposite films using CNFs as the reinforcement. The CNFs were physically extracted from softwood pulp without any chemicals involved during the process. The morphology, structure, optical, thermal and mechanical properties of the nanocomposite films were analyzed to evaluate the reinforcing effect of the CNFs as well as the miscibility and compatibility between CNFs and cellulose matrix.

## 2. Experimental

### 2.1. Materials

Dry softwood pulp with cellulose content above 95% was kindly provided by the Institute of Paper Science and Technology (Georgia Tech, USA). Microcrystalline cellulose (MCC) and other analytical grade chemical reagents were supplied by Chengdu Kelong Chemicals Co., Ltd. (Sichuan, China).

### 2.2. Preparation of CNFs

The preparation of CNFs from cellulose fibers was realized by sonication coupled with high shear homogenization. The dry softwood pulp board was cut into small pieces and soaked in distilled water for 10 h. Then, a disintegrator was used to evenly disperse softwood pulp in distilled water for 5 min. Subsequently, the cellulose suspension with a solid concentration of 2 wt% was treated with a horn type ultrasonic generator (JY99-IIDN, Scientz, China) for 30 min. The output power of the ultrasonic generator was set at 1200 W. After the ultrasonic pretreatment, the suspension was diluted with distilled water to a solid concentration about 0.5 wt%. The dispersion was further processed with a high shear homogenizer (T18, IKA, Germany) to isolate CNFs. The homogenization was conducted at a rotation speed of 20,000 rpm for 1 h. The yield of CNFs was determined by weighing a 10 mL aliquot of the suspension after standing overnight to dry (de Morais Teixeira et al., 2010). Yield (%) was calculated from the difference between initial and final weight. The CNFs were then separated from their aqueous suspension by centrifugation (4000 rpm, 10 min), and washed thoroughly with *N*,*N*-dimethylacetamide (DMAc) to exclude any traces of water. Finally, CNFs were redispersed in DMAc ultrasonically (400 W, 1 h) to form a CNFs suspension in DMAc.

### 2.3. Preparation of cellulose solution

MCC powder was firstly "activated" to help swell the cellulose for better dissolution. The activation process of cellulose was as follows: 8 g of MCC powder was swelled in 100 mL distilled water at 40 °C for 1 h. Subsequently, the MCC was filtered and subjected to solvent exchange with 100 mL methanol for 45 min, followed by solvent exchange with 100 mL anhydrous DMAc. All these processes were duplicated twice. To prepare a solvent solution of 8.0 wt% LiCl in DMAc, desired amounts of LiCl and DMAc were mixed in a 500 mL round-bottomed flask. The flask was sealed immediately to prevent moisture absorption. The mixture was then mechanically stirred for 1 h until the LiCl was completely dissolved. Finally, the activated MCC (8 g) was added to the LiCl/DMAc solution (200 g) under magnetic stirring at ambient condition until the solution became transparent.

### 2.4. Preparation of all-cellulose nanocomposite films

The preparation procedures of all-cellulose nanocomposite films were schemed in Fig. 1. A desired amount of CNFs suspended in DMAc was mixed with the as-prepared cellulose solution and stirred vigorously to form a homogenous mixture. The resultant viscous mixture was spread on glass plates and kept at ambient condition for 12 h to form a gel. The gels were washed thoroughly with distilled water and then air-dried at ambient temperature. Adhesive tapes were used to fix the gels on glass planes to prevent shrinkage during drying. Eventually, the films containing 0, 5, 10, 15, and 20 wt% CNFs were obtained and were denoted as CN0, CN5, CN10, CN15, and CN20, respectively.

### 2.5. Characterization

#### 2.5.1. Scanning electron microscope (SEM)

The suspensions of the cellulose fibers before and after the isolation process were air-dried. The obtained samples were coated with gold using a vacuum sputter coater and subsequently observed using SEM (Inspect F 50, FEI, USA) at 5 kV. ImageJ software was used to figure out the diameter distributions of more than 100 cellulose fibers or CNFs selected randomly from the SEM images. The surfaces and cross-sections (fractured in liquid nitrogen) of the nanocomposite films were observed by SEM at the accelerating voltage of 5 kV as well.

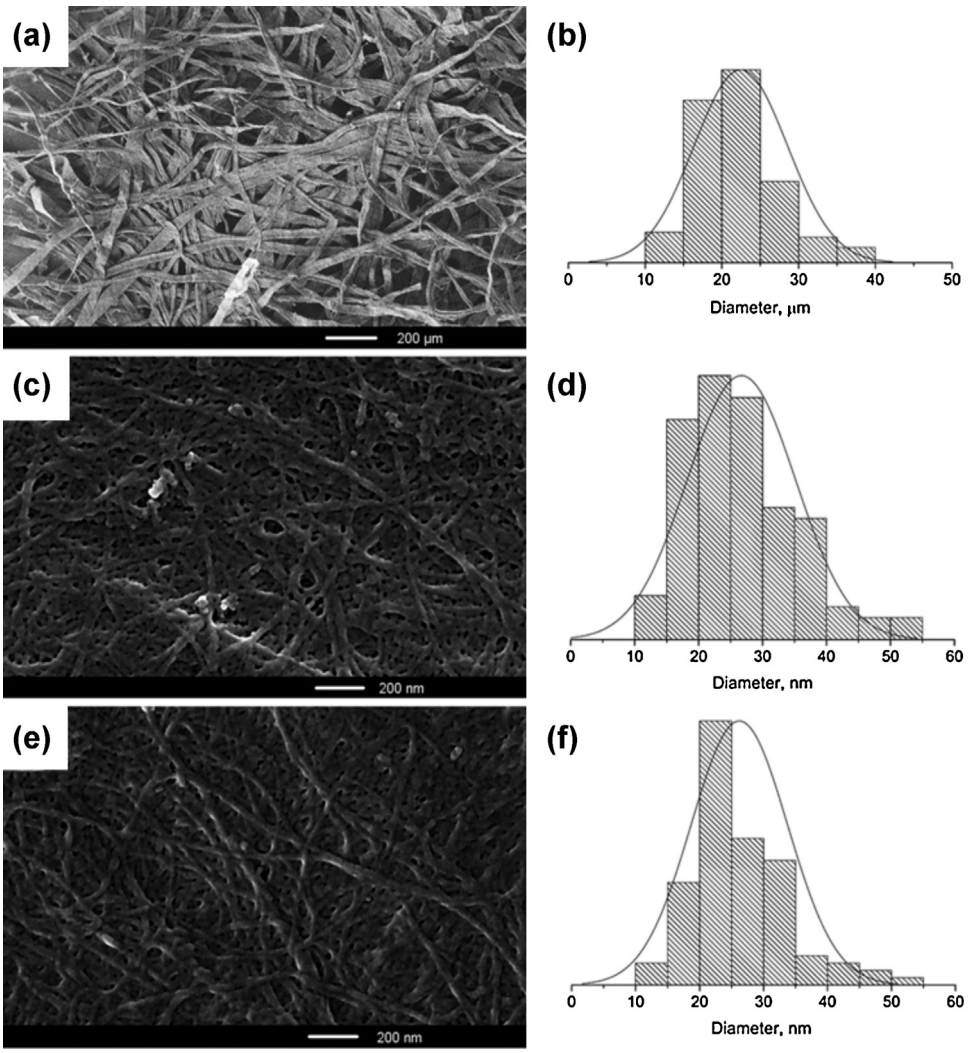


**Fig. 2.** SEM micrographs of the (a) pristine softwood cellulose fibers (the scale bar is 200 μm), (c) the obtained CNFs (the scale bar is 200 nm), (e) the treated CNFs (the scale bar is 200 nm); and diameter distribution of (b) pristine softwood cellulose fibers, (d) the obtained CNFs, (f) the treated CNFs.

*2.5.2. Mechanical properties measurements*

The mechanical properties of the composite films were measured on a universal testing machine (Instron 5567, USA) at a speed of 1 mm/min. The specimens of 50 mm in length and 10 mm in width were cut off from the composite films. Ten specimens were tested for each sample and the average values were reported.

*2.5.3. Optical transmittance measurements*

Optical transmittance (*Tr*) of all-cellulose composite films was measured with a UV–vis spectroscope (V-1800PC, Mapada, China) at the wavelength of 800 nm (Ma, Zhou, Li, Li, & Ou, 2011; Qi, Cai, Zhang, & Kuga, 2009). The thickness of the composite films was about 60 μm.

*2.5.4. X-ray diffraction studies*

X-ray diffraction (XRD) measurements were carried out using an X-ray diffractometer (X'Pert Pro MPD, Philips, Holland) with nickel filtered Cu Kα radiation (λ = 0.1540 nm) at 40 kV and 35 mA. The curve was recorded in the range of $2\theta = 5–40^\circ$ at a scanning speed of $2^\circ\ min^{-1}$. The total degree of crystallinity was calculated by the ratio of the crystalline scattering versus total scattering, while the crystallinity of individual crystal was calculated by the ratio of the individual crystalline scattering versus total scattering (Smole et al., 2003), and the formulae were as follows:

$$Cr = \frac{S_I + S_{II}}{S_I + S_{II} + Sa} \times 100\% \quad (1)$$

$$Cr_I = \frac{S_I}{S_I + S_{II} + Sa} \times 100\% \quad (2)$$

$$Cr_{II} = \frac{S_{II}}{S_I + S_{II} + Sa} \times 100\% \quad (3)$$

$$\frac{Cr_I}{Cr_{II}} = \frac{S_I}{S_{II}} \quad (4)$$

where *Cr* is the overall crystallinity of nanocomposite films; $C_I$ is the crystallinity of cellulose I crystal in the composite films; $Cr_{II}$ is the crystallinity of cellulose II crystal in the composite films; $S_I$ is the integrated area of cellulose I crystal peaks; $S_{II}$ is the integrated area of cellulose II crystal peaks; *Sa* is the integrated amorphous area of cellulose composites.

*2.5.5. Thermal gravimetric analysis (TGA)*

To assess the thermal stability of the composite films, thermal gravimetric analysis (TGA) was carried out using a thermogravimetric analysis equipment (STA 6000, Perkin Elmer, USA). Approximately 5 mg of each sample was placed in a platinum pan

and heated from 20 to 600 °C at a rate of 10 °C $min^{-1}$ under nitrogen atmosphere.

## 3. Results and discussion

### 3.1. Morphology of the cellulose fibers

Fig. 2(a) and (c) showed the SEM images of pristine softwood pulp fibers and as-prepared CNFs, respectively. It is evident that the cellulose fibers were almost completely disintegrated into CNFs after the individualization process. The diameter distributions of both pulp fibers and CNFs were statistically estimated using the software of ImageJ, which were shown in Fig. 2(b) and (d), respectively. The diameters of pristine softwood cellulose fibers were mainly distributed in the range of 15–30 μm, whereas most of the CNFs had diameters in the range of 15–40 nm. This is very close to the reported data of wood CNFs prepared by other nanofibrillation methods (Chen et al., 2011; Rodionova et al., 2013). The yield of CNFs for this process was calculated to be 97%, which was slightly higher than that (95%) for other isolation process of CNFs by ultrafine grinding (Jonoobi, Mathew, & Oksman, 2012). These results indicated that ultrasonic treatment coupled with high shear homogenization was very effective to produce CNFs.

To fabricate CNFs reinforced all-cellulose composites, CNFs have to be incorporated in the cellulose matrix solution. A question was raised that whether CNFs would be dissolved in the cellulose matrix solution or not. As is well recognized, cellulose needs to be activated prior to its dissolution in DMAc/LiCl solvent system. Without this pretreatment process, cellulose cannot be dissolved in LiCl/DMAc even after a long time of stirring (Dupont, 2003; Röder et al., 2002). In this study, no activation process was applied on the CNFs. Moreover, the optimum concentration of LiCl in the solvent mixture was in range between 5 and 9 wt% (Dawsey & McCormick, 1990). The concentration of LiCl in the solvent decreased from 8% to 4% after mixing the cellulose solution with CNFs suspension in DMAc, making it a poor solvent for cellulose. In addition, it was also kinetically unfavorable for the dissolution of CNFs since the solution had already contained a high concentration of dissolved cellulose from MCC. These explanations were experimentally supported by SEM imaging. CNFs were added into a DMAc/LiCl (96:4) solvent mixture and treated under the same condition for the composite film fabrication. The morphology and the diameter distribution of CNFs after treatment were shown in Fig. 2(e) and (f), respectively. The treated CNFs still kept their nanofibril morphology. The diameter distribution of treated CNFs was mainly in the range of 15–35 nm, which was similar to that of untreated CNFs (15–40 nm). These results suggested that CNF could not be dissolved in the matrix.

### 3.2. Mechanical properties and morphology of the nanocomposite films

The evaluation of mechanical properties could elucidate important information on the internal structure of the nanocomposite materials (Ma et al., 2011). Stress–strain curves of the all-cellulose nanocomposite films were shown in Fig. 3. The nanocomposite films exhibited significant improvements of mechanical properties with the addition of CNFs to the cellulose matrix. When the CNFs content increased from 0 wt% to 10 wt%, the tensile strength ($\sigma b$) increased from 61.56 MPa to 96.29 MPa. Thereafter, $\sigma b$ was nearly constant (as shown in Table 1). Evidently, the incorporation of CNFs into the cellulose matrix led to the strengthening of the materials. The CNFs tended to entangle with each other and form a fibrous network in the regenerated cellulose matrix. Due to the stiffness of CNFs and the strong interactions between CNFs and cellulose matrix through hydrogen bonds, it was possible that

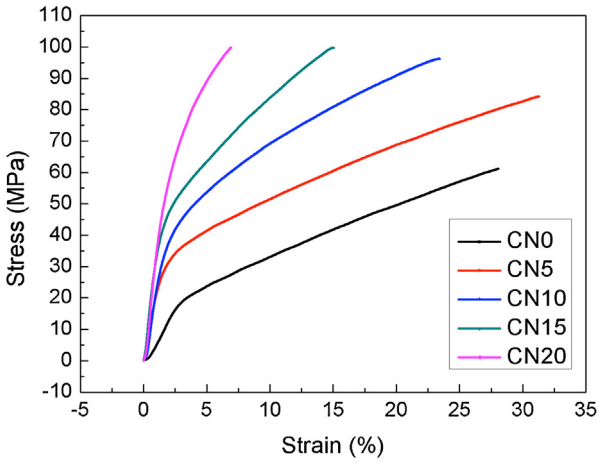


**Fig. 3.** Stress–strain curves of the all-cellulose nanocomposite films.

sufficient stress transfer could be realized from the relatively weak cellulose matrix to the strong CNFs as a result of good adhesion through the perfect interface.

However, when the CNFs content was higher than 10 wt%, the nanocomposite films exhibited almost constant tensile strength. As shown in Table 1, when the CNFs content was increased from 10 wt% to 20 wt%, the tensile strength increased slightly from 96.29 MPa to 99.92 MPa. It could be ascribed to the fact that the CNFs had a highly active surface and a large length/diameter ratio, which made them easily aggregate when the content of CNFs was high. This could induce phase separation and generate weak points in the composites. As a result, the tensile strength of the composite films did not show a remarkable enhancement when more than 10 wt% CNFs was added. Nevertheless, the increase of CNFs content significantly enhanced Young's modulus ($E$) of the films, from 0.76 GPa (CN0) to 4.16 GPa (CN20). However, the elongation at break ($\varepsilon$) decreased distinctly from 29.38% (CN0) to 6.93% (CN20). This result was well in line with previous reports on other all-cellulose nanocomposites using CNCs as the reinforcement (Ma et al., 2011; Qi et al., 2009). For example, Ma et al. (2011) discovered that the $\varepsilon$ of all-cellulose nanocomposites decreased from 13.89% to 2.11% when the content of CNCs increased from 0% to 25%. They ascribed this phenomenon to the phase separation as a result of CNCs aggregation at a high loading.

SEM images captured on both the surfaces and cross-sections of all-cellulose nanocomposite films were shown in Fig. 4. For pure regenerated cellulose film of CN0 in Fig. 4(a) and (f) and the nanocomposite film of CN5 in Fig. 4(b) and (g), relatively smooth surfaces and homogeneous cross-sections were observed, suggesting that the CNFs could be well dispersed in the regenerated cellulose matrix (Ma et al., 2011). However, the surfaces and cross-sections became increasingly rough as the content of CNFs further increased in the composites, indicating certain phase separation occurred as a result of CNFs aggregation (Qi et al., 2009).

### 3.3. Optical transmittance

The optical transparency is a useful criterion to assess the miscibility of the composite elements (Abdulkhani, Marvast, Ashori, & Karimi, 2013). The visible light transparency of the nanocomposite films was demonstrated in Fig. 5. The printed letters underneath the films could be observed for all films. However, the letters became blurred gradually with the increase of CNFs content. The optical transmittance ($Tr$) data at the wavelength of 800 nm for different films was listed in Table 1. The nanocomposite films

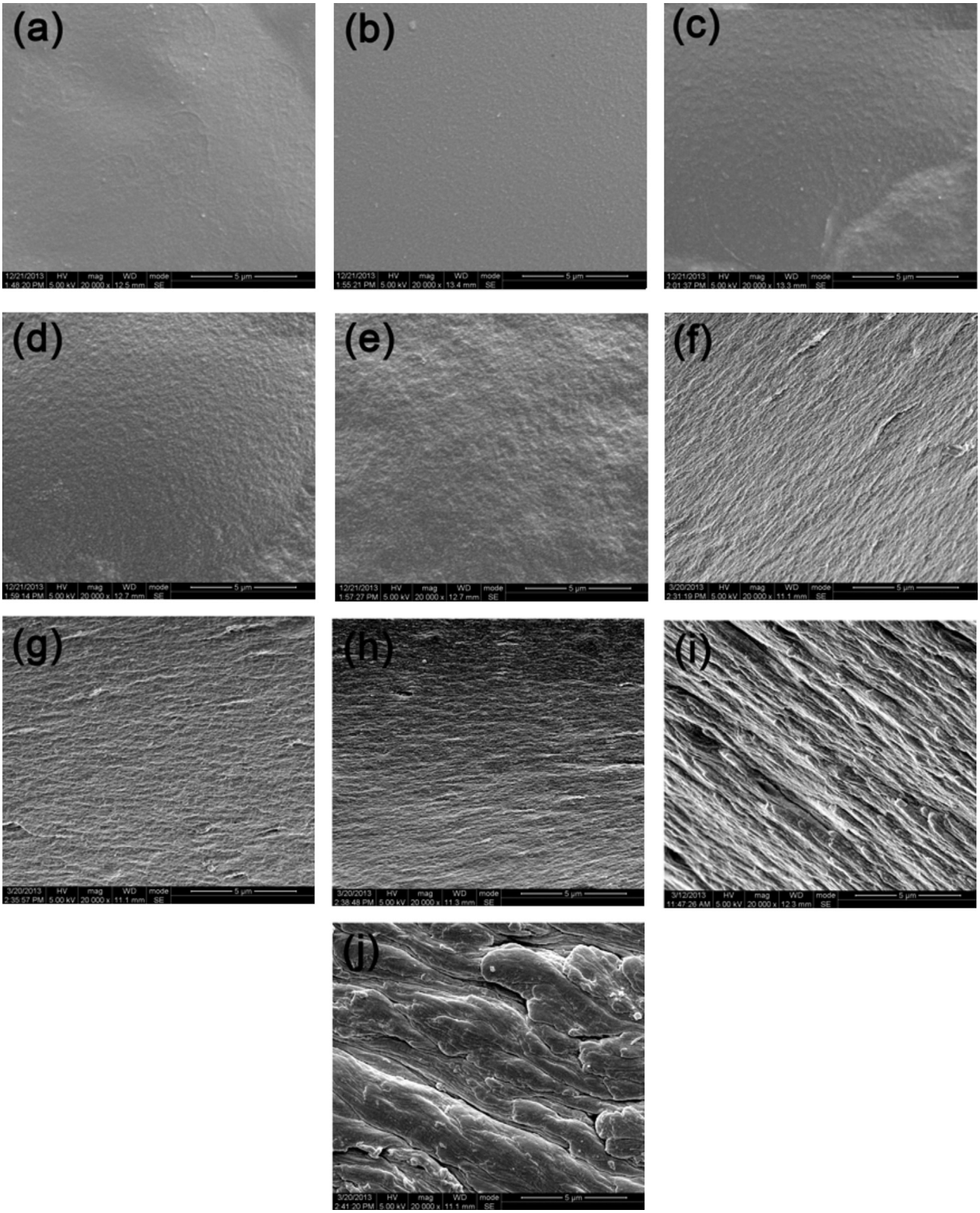


**Fig. 4.** The SEM images of surface (a–e) and cross-section (f–j) for all-cellulose nanocomposite films, CN0 (a and f); CN5 (b and g); CN10 (c and h); CN15 (d and i); CN20 (e and j).

with CNFs content of 5 wt% and 10 wt% exhibited high optical transparency with *Tr* values higher than 90%, indicating the good miscibility and compatibility (Qi et al., 2009). However, when the content of CNFs increased to 20 wt%, the *Tr* value of the nanocomposite films sharply decreased to 75.97%. As discussed earlier, CNFs would form aggregates when their content was high, which would induce phase separation and lead to serious light scattering at the cellulose matrix/CNFs aggregates interface. As a result, the optical transparency of the composites films deteriorated.

**Table 1**
Results of tensile testing, optical transmittance measurements, XRD studies, and TG analysis of the all-cellulose nanocomposite films.

| Samples | $\sigma b$ (MPa) | $E$ (GPa) | $\varepsilon$ (%) | $Tr$ (800 nm) | $Cr_I$ (%) | $Cr_{II}$ (%) | $T_d$ (°C) |
|---|---|---|---|---|---|---|---|
| CN0 | 61.56 | 0.76 | 29.38 | 96.44% | 0 | 41.22 | 279 |
| CN5 | 84.22 | 2.19 | 31.67 | 92.20% | 11.22 | 30.30 | 284 |
| CN10 | 96.29 | 2.91 | 25.34 | 89.44% | 16.31 | 24.98 | 292 |
| CN15 | 99.79 | 4.00 | 15.48 | 84.76% | 17.85 | 22.58 | 280 |
| CN20 | 99.92 | 4.16 | 6.93 | 75.97% | 20.75 | 19.42 | 276 |

Note: $\sigma b$, stress at failure; $E$, Young's modulus; $\varepsilon$, strain at failure; $Tr$, optical transmittance; $T_d$, initial decomposition temperature.

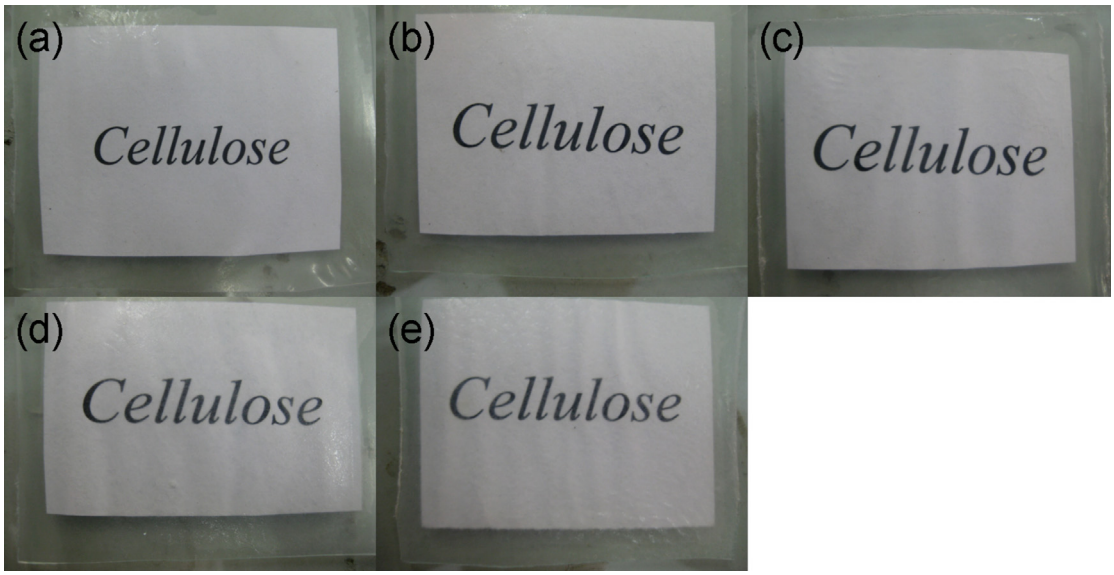


**Fig. 5.** The appearance of all-cellulose nanocomposite films. (a. CN0; b. CN5; c. CN10; d. CN15; e. CN20).

### 3.4. X-ray diffraction (XRD)

The XRD patterns of the composite films were shown in Fig. 6. The highest scattering intensity of the pure regenerated cellulose film was at the angle of 20.4°, indicating the crystal type of cellulose II (Gindl & Keckes, 2005). Whereas, CNFs showed the highest scattering intensity at 22.5° which corresponded to cellulose I crystal type (Ma et al., 2011). The XRD patterns of the composite films seemed to be overlapped patterns of both cellulose I and cellulose II crystals, analogous to other reports on all-cellulose composite films using the LiCl/DMAc solution system (Gindl & Keckes, 2005; Gindl & Keckes, 2007). The distinct shoulder at the scattering angle $2\theta = 22.5°$ indicated the presence of cellulose I crystal (2 0 0 planes) in the composite films. Moreover, as shown in Table 1, the content of cellulose I ($Cr_I$) in the films increased with the increase of initial proportion of CNFs from 5% to 20%. Meanwhile, the crystallinity of cellulose II ($Cr_{II}$) decreased from 41.22% to 19.42%. The overall crystallinity ($Cr$) of the all-cellulose nanocomposite films was nearly constant in the range of 40–42%. The increase of CNFs content would give rise to more cellulose I in the nanocomposite films, but the aggregation and phase separation of CNFs induced by the increasing CNFs content would lead to a decrease in the crystallinity of cellulose II ($Cr_{II}$) (Qi et al., 2009). As a result, the overall crystallinity was almost the same for the films with different CNFs concentrations.

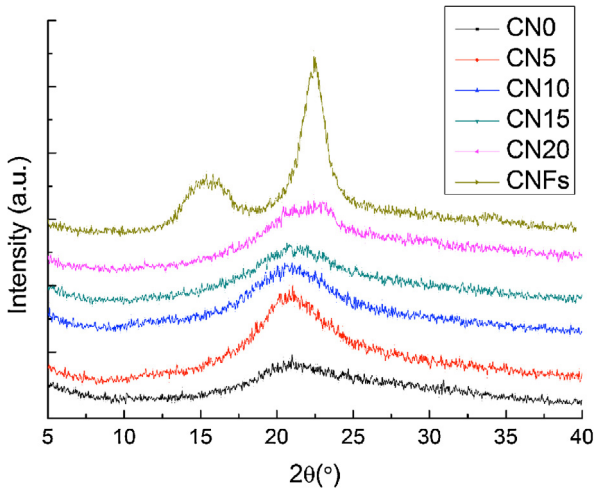


**Fig. 6.** X-ray diffraction patterns of CNFs and all-cellulose nanocomposite films.

### 3.5. Thermal stability

The TG curves of all-cellulose nanocomposite films were shown in Fig. 7. The initial slight mass loss (about 6%) was due to the evaporation of water existed in cellulose (Cabrales & Abidi, 2010; Ramiah, 1970). The initial decomposition temperatures ($T_d$) of the all-cellulose nanocomposite films were listed in Table 1. As expected, the $T_d$ of CN5 and CN10 nanocomposite films was higher than that of the CN0 film, suggesting CNFs could increase the thermal stability of the nanocomposite films due to the high compatibility between fillers and matrix (Ma et al., 2011). However, $T_d$ decreased from 292 °C to 276 °C when the content of filler increased from 10 wt% to 20 wt%. This could be ascribed to the phase separation as a result of CNFs aggregation.

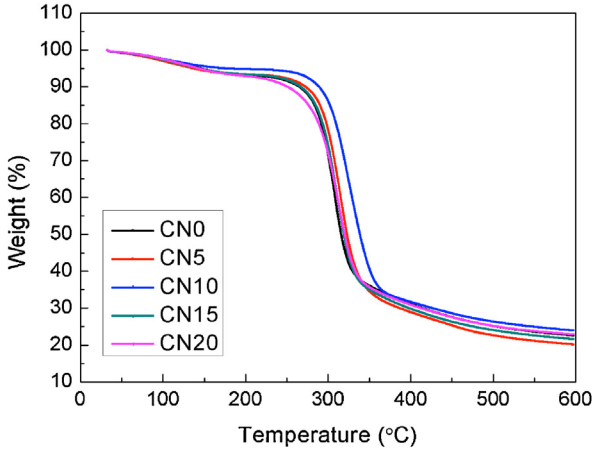


**Fig. 7.** TG curves of all-cellulose nanocomposite films.

## 4. Conclusions

A suspension of CNFs with diameters around 15–40 nm was successfully extracted from softwood pulp via simple physical methods. Self-reinforced all-cellulose nanocomposite films were fabricated using CNFs as fillers and regenerated cellulose as the matrix. CNFs exhibited a great reinforcing effect to cellulose matrix. The tensile strength, Young's modulus and the thermal stability of cellulose composites could be significantly improved when the content of CNFs was less than 10 wt%. However, CNFs could easily aggregate when the concentration of CNFs was high, resulting in a decline of the above mentioned properties. The advantages of biodegradability, high strength, and high optical transparency for the all-cellulose nanocomposite films will make them promising "green" materials in our future life.

## Acknowledgements

We are grateful to Natural Science Foundation of China (51303112 and 51203105) and Young Scholar Fund of Sichuan University (2012SCU11074) for financial support of this work. Mr. Sudhir Sharma from School of Chemical and Biomolecular Engineering at Georgia Tech is gratefully acknowledged for his contributions to the English improvement of this paper.

## References

Abdulkhani, A., Marvast, E. H., Ashori, A., & Karimi, A. N. (2013). Effects of dissolution of some lignocellulosic materials with ionic liquids as green solvents on mechanical and physical properties of composite films. *Carbohydrate Polymers*, *95*, 57–63.

Abe, K., Iwamoto, S., & Yano, H. (2007). Obtaining cellulose nanofibers with a uniform width of 15 nm from wood. *Biomacromolecules*, *8*, 3276–3278.

Abe, K., & Yano, H. (2012). Cellulose nanofiber-based hydrogels with high mechanical strength. *Cellulose*, *19*, 1907–1912.

Abraham, E., Deepa, B., Pothen, L. A., Jacob, M., Thomas, S., Cvelbar, U., et al. (2011). Extraction of nanocellulose fibrils from lignocellulosic fibres: A novel approach. *Carbohydrate Polymers*, *86*, 1468–1475.

Abraham, E., Deepa, B., Pothen, L. A., Cintil, J., Thomas, S., John, M. J., et al. (2013). Environmental friendly method for the extraction of coir fibre and isolation of nanofibre. *Carbohydrate Polymers*, *92*, 1477–1483.

Abraham, E., Deepa, B., Pothan, L. A., John, M., Narine, S. S., Thomas, S., et al. (2013). Physicomechanical properties of nanocomposites based on cellulose nanofibre and natural rubber latex. *Cellulose*, *20*, 417–427.

Azeredo, H. M. C., Mattoso, L. H. C., Wood, D., Williams, T. G., Avena-Bustillos, R. J., & Mchugh, T. H. (2009). Nanocomposite edible films from mango puree reinforced with cellulose nanofibers. *Journal of Food Science*, *74*, 31–35.

Cabrales, L., & Abidi, N. (2010). On the thermal degradation of cellulose in cotton fibers. *Journal of Thermal Analysis and Calorimetry*, *102*, 485–491.

Cervin, N. T., Andersson, L., Ng, J. B. S., Olin, P., Bergström, L., & Wågberg, L. (2013). Lightweight and strong cellulose materials made from aqueous foams stabilized by nanofibrillated cellulose. *Biomacromolecules*, *14*, 503–511.

Chen, W., Yu, H., Liu, Y., Chen, P., Zhang, M., & Hai, Y. (2011). Individualization of cellulose nanofibers from wood using high-intensity ultrasonication combined with chemical pretreatments. *Carbohydrate Polymers*, *83*, 1804–1811.

Dagnon, K. L., Shanmuganathan, K., Weder, C., & Rowan, S. J. (2012). Water-triggered modulus changes of cellulose nanofiber nanocomposites with hydrophobic polymer matrices. *Macromolecules*, *45*, 4707–4715.

Dawsey, T. R., & McCormick, C. L. (1990). The lithium chloride/dimethylacetamide solvent for cellulose: A literature review. *Journal of Macromolecular Science, Part C: Polymer Reviews*, *30*, 405–440.

de Morais Teixeira, E., Corrêa, A. C., Manzoli, A., de Lima Leite, F., de Oliveira, C. R., & Mattoso, L. H. C. (2010). Cellulose nanofibers from white and naturally colored cotton fibers. *Cellulose*, *17*, 595–606.

Dupont, A.-L. (2003). Cellulose in lithium chloride/*N, N*-dimethylacetamide, optimisation of a dissolution method using paper substrates and stability of the solutions. *Polymer*, *44*, 4117–4126.

Gao, C., Yu, L., Liu, H., & Chen, L. (2012). Development of self-reinforced polymer composites. *Progress in Polymer Science*, *37*, 767–780.

Gindl, W., & Keckes, J. (2005). All-cellulose nanocomposite. *Polymer*, *46*, 10221–10225.

Gindl, W., & Keckes, J. (2007). Drawing of self-reinforced cellulose films. *Journal of Applied Polymer Science*, *103*, 2703–2708.

Gindl-Altmutter, W., Keckes, J., Plackner, J., Liebner, F., Englund, K., & Laborie, M.-P. (2012). All-cellulose composites prepared from flax and lyocell fibres compared to epoxy–matrix composites. *Composites Science and Technology*, *72*, 1304–1309.

Huber, T., Müssig, J., Curnow, O., Pang, S., Bickerton, S., & Staiger, M. P. (2012). A critical review of all-cellulose composites. *Journal of Materials Science*, *47*, 1171–1186.

Jayaramudu, J., Siva Mohan Reddya, G., Varaprasad, K., Sadiku, E. R., Sinha Ray, S., & Varada Rajulu, A. (2013). Preparation and properties of biodegradable films from *Sterculia urens* short fiber/cellulose green composites. *Carbohydrate Polymers*, *93*, 622–627.

Jonoobi, M., Mathew, A. P., Abdi, M. M., Makinejad, M. D., & Oksman, K. (2012). A comparison of modified and unmodified cellulose nanofiber reinforced polylactic acid (PLA) prepared by twin screw extrusion. *Journal of Polymers and the Environment*, *20*, 991–997.

Jonoobi, M., Mathew, A. P., & Oksman, K. (2012). Producing low-cost cellulose nanofiber from sludge as new source of raw materials. *Industrial Crops and Products*, *40*, 232–238.

Leitner, J., Hinterstoisser, B., Wastyn, M., Keckes, J., & Gindl, W. (2007). Sugar beet cellulose nanofibril-reinforced composites. *Cellulose*, *14*, 419–425.

Ma, H., Zhou, B., Li, H., Li, Y., & Ou, S. (2011). Green composite films composed of nanocrystalline cellulose and a cellulose matrix regenerated from functionalized ionic liquid solution. *Carbohydrate Polymers*, *84*, 383–389.

Ma, S., Xue, X., Yu, S., & Wang, Z. (2012). High-intensity ultrasound irradiated modification of sugarcane bagasse cellulose in an ionic liquid. *Industrial Crops and Products*, *35*, 135–139.

Madera-Santana, T. J., Soto Valdez, H., & Richardson, M. O. W. (2013). Influence of surface treatments on the physicochemical properties of short sisal fibers: Ethylene vinyl acetate composites. *Polymer Engineering & Science*, *53*, 59–68.

Nishino, T., Matsuda, I., & Hirao, K. (2004). All-cellulose composite. *Macromolecules*, *37*, 7683–7687.

Qi, H., Cai, J., Zhang, L., & Kuga, S. (2009). Properties of films composed of cellulose nanowhiskers and a cellulose matrix regenerated from alkali/urea solution. *Biomacromolecules*, *10*, 1597–1602.

Ramiah, M. V. (1970). Thermogravimetric and differential thermal analysis of cellulose, hemicellulose, and lignin. *Journal of Applied Polymer Science*, *14*, 1323–1337.

Röder, T., Potthast, A., Rosenau, T., Kosmsa, P., Baldinger, T., Morgenstern, B., et al. (2002). The effect of water on cellulose solutions in DMAc/LiCl. *Macromolecular Symposia*, *190*, 151–160.

Rodionova, G., Saito, T., Lenes, M., Eriksen, Ø., Gregersen, Ø., Kuramae, R., et al. (2013). TEMPO-mediated oxidation of Norway spruce and Eucalyptus pulps: Preparation and characterization of nanofibers and nanofiber dispersions. *Journal of Polymers and the Environment*, *21*, 207–214.

Sehaqui, H., Mushi, N. E., Morimune, S., Salajkova, M., Nishino, T., & Berglund, L. A. (2012). Cellulose nanofiber orientation in nanopaper and nanocomposites by cold drawing. *ACS Applied Materials and Interfaces*, *4*, 1043–1049.

Sehaqui, H., Salajkova, M., Zhou, Q., & Berglund, L. A. (2010). Mechanical performance tailoring of tough ultra-high porosity foams prepared from cellulose I nanofiber suspensions. *Soft Matter*, *6*, 1824–1832.

Smole, M. S., Peršin, Z., Kreže, T., Kleinschek, K. S., Ribitsch, V., & Neumayer, S. (2003). X-ray study of pre-treated regenerated cellulose fibres. *Materials Research Innovations*, *7*, 275–282.

Syverud, K., Chinga-Carrasco, G., Toledo, J., & Toledo, P. G. (2011). A comparative study of Eucalyptus and *Pinus radiata* pulp fibres as raw materials for production of cellulose nanofibrils. *Carbohydrate Polymers*, *84*, 1033–1038.

Takagi, H., & Asano, A. (2008). Effects of processing conditions on flexural properties of cellulose nanofiber reinforced "green" composites. *Composites: Part A*, *39*, 685–689.

Teixeira, E. M., Pasquini, D., Curvelo, A. A. S., Corradini, E., Belgacem, M. N., & Dufresne, A. (2009). Cassava bagasse cellulose nanofibrils reinforced thermoplastic cassava starch. *Carbohydrate Polymers*, *78*, 422–431.

Tonoli, G. H. D., Teixeira, E. M., Corrêa, A. C., Marconcini, J. M., Caixeta, L. A., Pereira-da-Silva, M. A., et al. (2012). Cellulose micro/nanofibres from Eucalyptus kraft pulp: Preparation and properties. *Carbohydrate Polymers*, *89*, 80–88.

Tonoli, G. H. D., Belgacem, M. N., Siqueira, G., Bras, J., Savastano, H., Jr., & Rocco Lahr, F. A. (2013). Processing and dimensional changes of cement based composites

reinforced with surface-treated cellulose fibres. *Cement and Concrete Composites*, *37*, 68–75.

Vallejos, M. E., Peresin, M. S., & Rojas, O. J. (2012). All-cellulose composite fibers obtained by electrospinning dispersions of cellulose acetate and cellulose nanocrystals. *Journal of Polymers and the Environment*, *20*, 1075–1083.

Xiong, R., Zhang, X., Tian, D., Zhou, Z., & Lu, C. (2012). Comparing microcrystalline with spherical nanocrystalline cellulose from waste cotton fabrics. *Cellulose*, *19*, 1189–1198.

Xu, X., Liu, F., Jiang, L., Zhu, J. Y., Haagenson, D., & Wiesenborn, D. P. (2013). Cellulose nanocrystals vs. cellulose nanofibrils: A comparative study on their microstructures and effects as polymer reinforcing agents. *Applied Materials and Interfaces*, *5*, 2999–3009.

Zhao, J., Zhang, W., Zhang, X., Zhang, X., Lu, C., & Deng, Y. (2013). Extraction of cellulose nanofibrils from dry softwood pulp using high shear homogenization. *Carbohydrate Polymers*, *97*, 695–702.